Simulation and experimental study of a random neutron analyzing system with ^{252}Cf neutron source

FENG Peng* LIU Siyuan WEI Biao JIN Jing MI Deling

Key Laboratory of Opto-electronics Technology & System, Ministry of Education, Chongqing University, Chongqing 400044, China

Abstract Experiments were performed on a high-speed online random neutron analyzing system (HORNA system) with a ^{252}Cf neutron source (up to 1 GHz sampling rate and 3 input data channel), to obtain time- and frequency-dependent signatures which are sensitive to changes in the composition, fissile mass and configuration of the fissile assembly. The data were acquired by three high-speed synchronized acquisition cards at different detector angles, source-detector distances and block sizes. According to the relationship between ^{252}Cf source and the ratio of power spectral density, R_{psd}, all the signatures were calculated and analyzed using correlation and periodogram methods. Based on the results, the simulated autocorrelation functions were utilized for identifying different fissile mass with Elman neural network. The experimental results show that the R_{psd} almost remains at constant amplitude in frequency range of 0–100 MHz, and is only related to the angle and source-detector distance. The trained Elman neural network is able to distinguish the characteristics of autocorrelation function and identify different fissile mass. The average identification rate reached 90% with high robustness.

Key words ^{252}Cf Neutron source, Random neutron pulse signal, Ratio of power spectral density, Elman neural network, Fissile material identification

1 Introduction

The interaction between neutrons and nuclear material can be used to unveil the inner structure of fissile material[1-3]. By analyzing the random neutron pulse signals from the fission induced by ^{252}Cf neutrons, one obtains a series of parameters, such as autocorrelation, cross correlation, auto/cross power spectrum and ratio of power spectral density. Being sensitive to changes in composition, mass, and configuration of the fissile assembly, the parameters are very useful in obtaining reactivity of the fission system or fission materials.

A great deal of research efforts have been made during the past 20 years. Mihalczo J T *et al*[4] have been doing the neutron pulse sequence detection and analysis using a ^{252}Cf neutron source since mid 1990s, based on ^{252}Cf source-driven noise analysis method[5], which is also known as power spectral density analysis method[6,7]. In China, studies in this field of research are in the startup stage, and limited to low speed (10 –100 MHz sampling rate), low count rate (10^2–10^4 s^{-1}) and non-realtime analysis and processing, while most of high-speed and high count rate spectrum analyses were done with Monte Carlo simulation package[8,9].

In this paper, we focus on the calculation and analysis of various spectra of three-channel neutron pulse signals using periodogram and block correlation method. All the neutron pulse data are acquired by a high-speed online random neutron analyzing system (HORNA system) developed at our laboratory[10-12]. The data are collected at different angles, distances and block sizes at the sampling rate of 1GHz. The physical significance of random neutron signals is discussed. According to the linear relationship between the fissile mass and integrated autocorrelation function[5], the possibility of identifying different fissile masses is explored in temporal domain using the Elman neural network, where the characteristics of autocorrelation function is a key input variable.

Supported by Natural Science Foundation Project of CQ (CSTC2009BB2188) and Fundamental Research Funds for Central Universities (No. CDJXS10120013)

* Corresponding author. *E-mail address:* coe-fp@cqu.edu.cn

Received date: 2010-05-20

Elman Neural Network (ENN)[13] is a type of partial recurrent neural network, which consists of two-layer back propagation networks with an additional feedback connection from the output of the hidden layer to its input layer. The advantage of this feedback path is that it allows ENN to recognize and generate temporal and spatial patterns[14]. This means that interrelations between the current input and internal states are processed to produce the output and represent relevant information in the internal states after training[14]. Combining it with our autocorrelation function, different fissile masses can be identified in the time domain, instead of the frequency domain.

In Section 2 we give a brief description of this ^{252}Cf-based HORNA system and key characteristics of correlation functions. In Section 3, we present how to calculate and analyze the rate of power spectral density for the HORNA system. In this work, we also focused on acquiring and processing the data from the experiment with different angles, distances and block sizes. The identification of different fissile masses by Elman neural network is presented Section 4, with descriptions about how to generate the simulated autocorrelation data and how to train and integrate the data into the distributed Elman neural network, and the resulted identification rates are compared.

2 System overview

The ^{252}Cf-source-driven noise analysis method has been evolved as a combination of randomly pulsed neutron measurements and Rossi-α measurements[15]. A ^{252}Cf source is used to stimulate events in the fissile material and the subsequent emission of neutrons and gamma rays from the fissile system are measured with two or more detectors. A typical block diagram for this measurement is shown in Fig.1a. The ^{252}Cf source, contained in an ionization chamber, provides a pulse signal for each spontaneous fission event. The source ionization detector is designated as Detector l and the radiation detectors are designated as Detectors 2, 3 etc. The pulses from the source and detectors are acquired over a large time interval (block size) of 512, 1024, 2048 and 4096 time bins that can be as short as 1 ns. The source and detector signals are correlated with each other to obtain a wide variety of time- and frequency-dependent parameters/signatures. From the signatures the moments or reduced moments of the count events and the Feynrnan variance are obtained. Specific parameters of reactivity of the fissile material, the prompt neutron decay constant and other physical parameters can be derived, too.

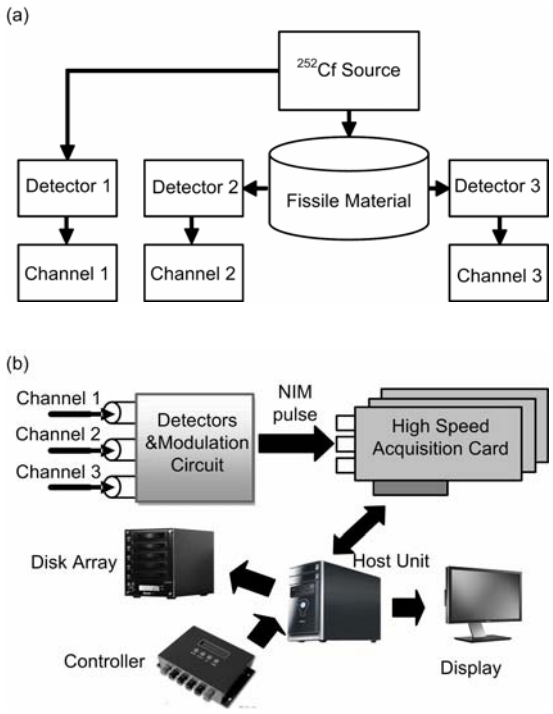

Fig.1 Block diagram and schematics of the HORNA system.

Based on this method, we constructed an HORNA system[10,11], with its basic architecture shown in Fig.1b. It has three input channels: Channel 1 of the ^{252}Cf source detector, and Channels 2 and 3 of the detectors to detect neutrons from the fissile material. The detector signals from neutrons emitted from the ^{252}Cf source and fissile material are sent to modulation circuit that performs constant fraction discrimination (CFD) to produce well-defined NIM level pulses. The, NIM pulses from the three channels are synchronously sampled at 1 GHz sampling rate. A time bin having a signal is represented by “1”, and “0” otherwise. The pulses are inputted to high-speed acquisition card residing in a high-performance Windows-based host unit. Data acquisition is controlled by the software that includes a graphical user interface, digital signal processing algorithms, data archival, and a device driver for the acquisition card. All signal processing are performed online and executed on the host unit.

Through the HORNA system, three signal sequences formed by “0” and “1” that reflect the time

distribution of the source or fission-induced neutrons can be obtained. These adjacent time intervals form a series of data blocks, with block sizes of 512, 1024, 2048 and 4096. All the data blocks are processed through periodogram or block correlation analysis method, and over twenty time- and frequency-dependent signatures can be obtained, such as autocorrelation function of each channel (R_{11}, R_{22}, R_{33}), cross correlation function between two channels(R_{12}, R_{13}, R_{23}); multiplicity of each channel (M_1, M_2, M_3); auto power spectral density of each channel (G_{11}, G_{22}, G_{33}), cross power spectral density between two channels(G_{12}, G_{13}, G_{23}), ratio of power spectral density (R_{psd}), the reactivity of nuclear fissile material (K_{eff}), prompt neutron decay constant(α), and other physical parameters. Typical signatures are shown in Fig.2.

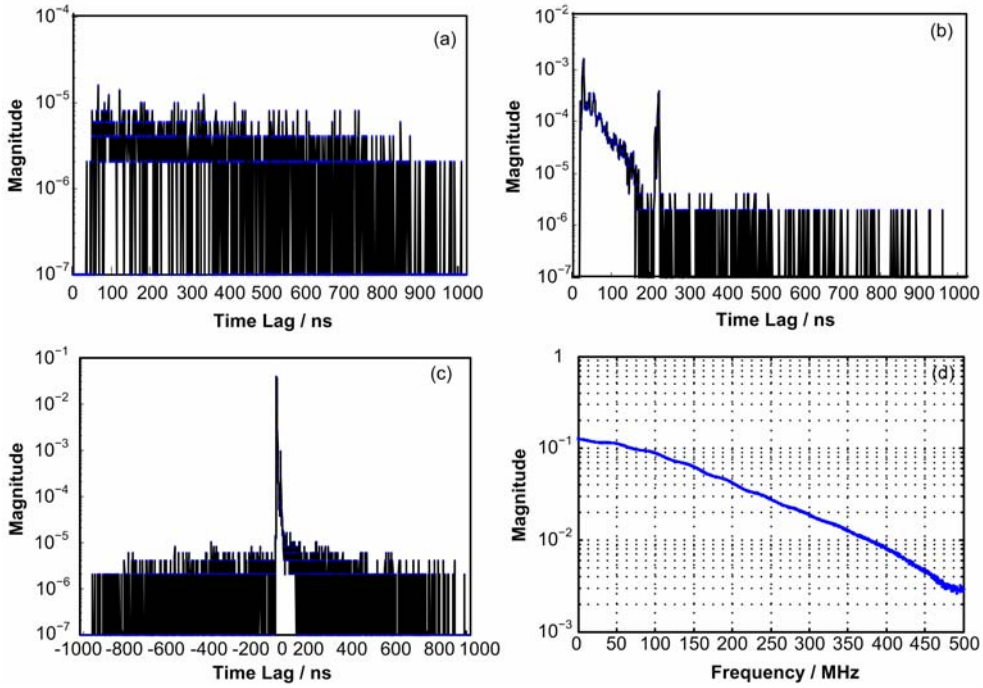

Fig.2 Plots of some signatures of the ^{252}Cf measurement system.

The autocorrelation function of a detector channel can be sensitive to fissile mass. As an example one of the detector autocorrelation functions (R_{22}) is shown in Fig.3.

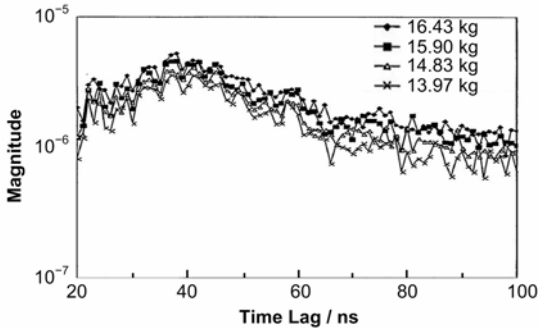

Fig.3 Autocorrelation function of Ch. 2 for ^{235}U of different masses.

Approximately, the R_{22} decreases exponentially from 40 to 100 ns. This means that R_{22} has a slight dependence on fissile mass, though this is not seen prior to 20 ns due to the dead time of the detection system as shown in Figs.2a and 2b. The detector autocorrelation functions were integrated over the time and the total correlated counts for the detectors were obtained with different fissile mass, as given in Table 1. The integral of the total correlated counts increases with the fissile mass. The integral of the autocorrelation functions increases by about 13% from 13.97 to 16.43 kg of ^{235}U. It can be inferred that the differences of autocorrelation function's amplitude may reflect different fissile mass and this differences can be potentially used in the identification process.

Table 1 Integral of detector autocorrelation for different fissile masses.

Fissile mass / kg	13.97	14.83	15.90	16.43
R22	0.0825	0.0870	0.0917	0.0959
R33	0.0836	0.0834	0.0941	0.0972

3 Calculation and analysis of R_{psd}

3.1 The ratio of power spectral density

Among all the parameters, R_{psd} is independent of uncorrelated background, detector types and detection efficiency[4]. R_{psd} is only related to characteristics of the ^{252}Cf source and the relative position between the detectors when fissile material is not involved in. If all detectors are fixed before experiments, R_{psd} shall be a constant for a given ^{252}Cf source. R_{psd} is defined as:

$$R_{psd}(\omega)=\frac{G_{12}^{*}(\omega)G_{13}(\omega)}{G_{11}(\omega)G_{23}(\omega)} \quad (1)$$

where * means complex conjugation, $G_{11}(\omega)$ is the auto power spectral density of Channel 1, $G_{12}(\omega)$ is the cross power spectral density between Channels 1 and 2, and so are $G_{13}(\omega)$ and $G_{23}(\omega)$. In Eq.(1), detection efficiencies in the numerator and denominator are cancelled much in the same way as in beta-gamma coincidence counting methods, and the frequency response of the detection systems is cancelled[4,5], too. This has been proved by measurements of the past 20 years, in which the same value of R_{psd} no matter what kind of detectors were used[16].

As the frequency increases, and the correlation decreases, R_{psd} may maintain constant, and reflect the system performance effectively. So, R_{psd} can serve as a key indicator in the calibration system without fissile material. As calculated from the plot in Fig.4, the mean value of R_{psd} is 0.6568±0.01278 for frequencies of up to 100 MHz, i.e. R_{psd} almost keeps steady and the result coincides with the theoretical analysis. Because of the decreased coherence, R_{psd} decreases with increasing frequencies to about 0 at 500 MHz.

3.2 Experimental

To verify the effectiveness of the HORNA systems, a calibration without fissile material was carried out with a ^{252}Cf source of 2.1×10^{4} s^{-1} in fission rate and at sampling rate of 1 GHz. The detector positions are shown in Fig.5, where $\alpha=\pi/6$, $9\pi/24$, $\pi/2$ and π is the angle between Detectors 2 and 3, and L=15 and 30 cm is the source-detector distance. To analyze the impact of different calculation methods on the final results, we changed the blocksize (512, 1024, 2048 and 4096) to calculate R_{psd} with the block correlation and periodogram methods. The calculated R_{psd} (mean±SD) of up to 100 MHz are given in Table 2.

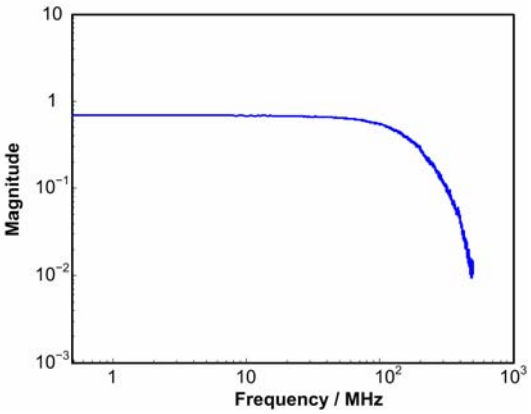

Fig.4 R_{psd} values in logarithmic coordinate.

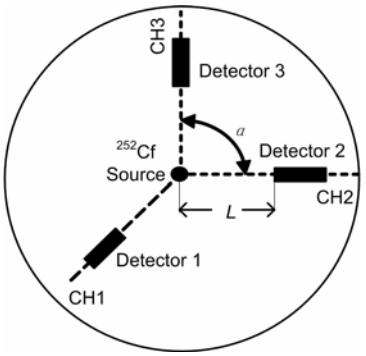

Fig.5 Position of the detectors.

Table 2 shows that for a given set of experiments, whatever the angle and distance are, R_{psd} remains steady at low-frequencies, and the difference between the results of block correlation method and periodogram method is about 10^{-3} under the same L, α and blocksize. So the choice of different calculation methods affects little, but the change of detector angle α brings obvious impact on the R_{psd}. Mihalczo J T *et al*[16] showed that R_{psd} is only related to α and L for a given ^{252}Cf neutron source, no matter what kind of detectors are used. Its value is inversely proportional to L and has complicated trigonometric function relationship with α. From Table 2, the R_{psd} increases with α, with a maximum at $9\pi/24$ due to anisotropy of the ^{252}Cf source.

All these show that the calibration results agree with the theoretical analysis that R_{psd} reflects the key feature of ^{252}Cf source. A larger block size increases the R_{psd} accordingly. In a small size block with a low rate ^{252}Cf fission source and a large time interval

between two pulses signals, there may be only one pulse, making it hard to describe the correlation between the signals. In a big-size block, however, there can be more pulses strengthening the correlation, and the source signal characteristics can be fully depicted. If block size increases to cover the interval between two adjacent pulses, the R_{psd} should remain constant. Therefore, statistics of the time interval should be analyzed and different block sizes and source intensities be chosen for a measurement.

Table 2 Result of the calibration experiments

No.	α / rad	L / cm	Block Correlation Method				Periodogram Method			
			512	1024	2048	4096	512	1024	2048	4096
1	π/2	30	0.6443±0.0125	0.6568±0.0127	0.6626±0.0127	0.6657±0.0129	0.6467±0.0157	0.6603±0.0203	0.6666±0.0133	0.6703±0.0189
2	π/2	30	0.6309±0.0215	0.6593±0.0257	0.6845±0.0287	0.6851±0.0335	0.6415±0.0201	0.6567±0.0299	0.6778±0.0295	0.6837±0.0353
3	π/2	30	0.6356±0.0382	0.6695±0.0436	0.6910±0.0605	0.7092±0.0809	0.6635±0.0337	0.6781±0.0406	0.6830±0.0674	0.6989±0.0712
4	π	15	0.7062±0.0209	0.7149±0.0281	0.7187±0.0153	0.7210±0.0159	0.7026±0.0210	0.7159±0.0254	0.7236±0.0147	0.7219±0.0156
5	π	15	0.6975±0.0149	0.7090±0.0204	0.7059±0.0298	0.7076±0.0120	0.7012±0.0136	0.7028±0.0181	0.7054±0.0311	0.6809±0.0117
6	π/6	15	0.4487±0.0097	0.4743±0.0112	0.4883±0.0134	0.4954±0.0171	0.4449±0.0089	0.4701±0.0122	0.4892±0.0143	0.4983±0.0101
7	9π/24	15	0.7863±0.0078	0.8326±0.0094	0.8559±0.0098	0.8648±0.0106	0.7878±0.0077	0.8362±0.0101	0.8618±0.0098	0.8691±0.0095

4 Elman neural network-based identification for nuclear signal

4.1 Elman neural network

Based on the linearity between fissile mass and the value of integral of autocorrelation function, we used the Elman neural network method for identifying the nuclear signal. The Elman neural network is a feed-forward network with two layers (Fig.6).

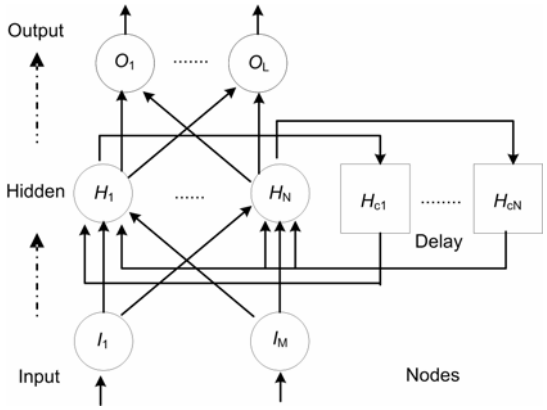

Fig.6 Architecture of the Elman neural network.

This type of network differs from conventional ones in that the input layer has a recurrent connection with the hidden one. Therefore, at each time step the output values of the hidden units are copied to the input ones, which store them and use them for the next time step. This process allows the network to memorize some information from the past. In this way periodicity of the patterns can be better detected[13].

The activation functions for the hidden layer and output layer are tangent sigmoid function (tansig) and linear function (purelin), respectively, expressed in the following equations:

$$\text{Tansig: } \Phi_\sigma(n) = 2/(1+e^{-2\sigma n}) - 1$$

$$\text{Purelin: } \Phi(n) = n$$

where the parameter σ will be set to 1. The learning rule we used is the error back-propagation algorithm[14]. The learning rate λ can be chosen.

4.2 Design and training of the distributed Elman neural network

Here we chose R_{22} or R_{33} as input, and the normalized fissile mass u as output. Due to the dead time of this system described in Section 2, we chose the values of autocorrelation function just between 20 ns and 99 ns as the input to the neural network, which means that the nodes of input are 80.

For a given number of samples, the network will not fully reflect the signal characteristics if the network parameters are not enough, or too many. And inputting the 80 values of R_{22} or R_{33} directly will make the network complex with increased training samples and time[12]. We divided the signal into segments and distributed them to sub-networks, so as

to construct a distributed neural network to identify the signal partly (Fig.7). The distributed neural network contains 16 sub-neural networks (Elman network), and the number of input node for each subnet was 5, and the outputs of the 16 sub-network were averaged.

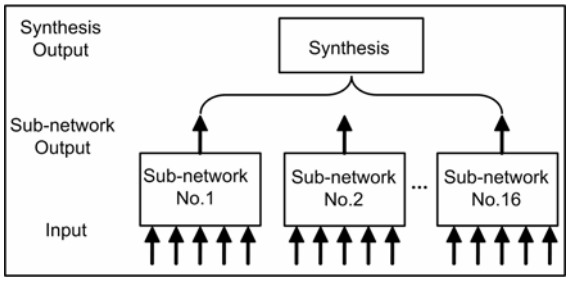

Fig.7 Schematic diagram of distributed Elman network.

As the autocorrelation function decays exponentially, and the integration of autocorrelation function between different fissile mass is of approximate linearity (Section 2), we multiplied the autocorrelation result by a random coefficient generated from a standard normal distribution sequence to get different samples, as shown in Eq.(2):

$$\boldsymbol{y} = \frac{1}{2 * |\max(\boldsymbol{x})|} * \boldsymbol{x} + b \tag{2}$$

where $\boldsymbol{y}$ is the coefficient sequence, $\boldsymbol{x}$ is the standard normal distribution sequence, and b is the weight applied to distinguish the signal amplitude. In this way, 10 sets of signals which include 4 kinds of fissile mass were generated. Five sets of the signals were used as the training samples and the others as the test samples. Fig.8 shows one of the simulated signals.

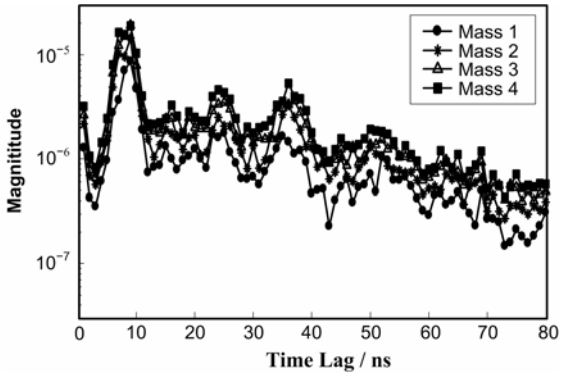

Fig.8 A simulated autocorrelation function with different fissile mass.

The normalized mass output is given by Eq.(3):

$$\overline{u_i} = \frac{u_i - u_i^{\min}}{u_i^{\max} - u_i^{\min}} \qquad i = 1,2,3,4 \tag{3}$$

where u_i (i=1,2,3,4) denotes the fissile masses as the neural network output, $u_i^{\min}$ and $u_i^{\max}$ are the minimum and maximum of the i^{th} fissile mass. $\overline{u_i}$ is the i^{th} normalized mass output which belongs to [0,1] and 4 kinds of predefined fissile mass can be written as [0, 0.33, 0.66, 1].

4.3 The simulation results

All the 16 sub-networks were trained with R_{22} or R_{33}. After 1500 iteration steps, the training was terminated when the convergence error reached 0.01. The identification results are shown in the Fig.9.

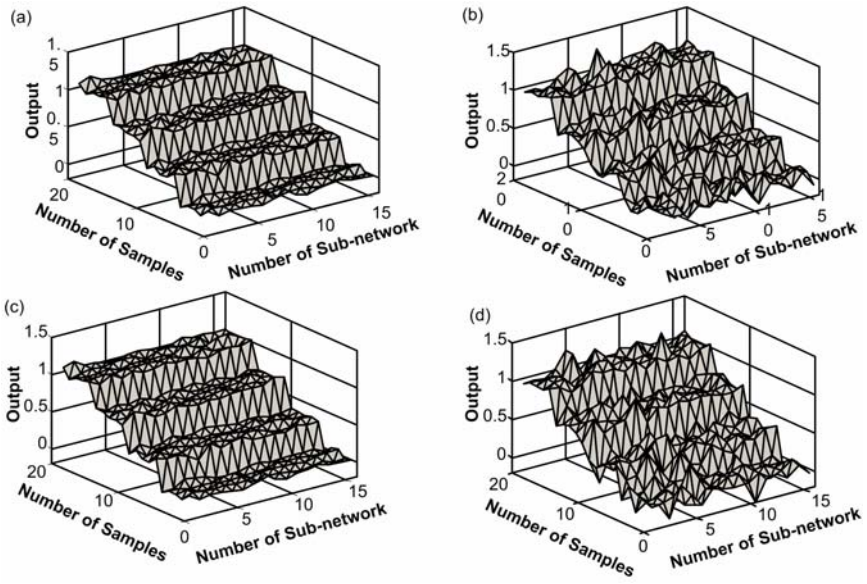

Fig.9 Identification results of R_{22} (a, b) and R_{33} (c, d).

Table 3 Result of identification for sub-networks

Rate	R_{22}					R_{33}				
	S_1	S_2	S_3	S_4	S_5	S_1	S_2	S_3	S_4	S_5
Mass 1	87.5	81.25	81.25	81.25	100	81.25	81.25	81.25	81.25	81.25
Mass 2	75	93.75	87.50	100	87.50	75	75	75	75	75
Mass 3	93.75	93.75	81.25	93.75	87.50	93.75	93.75	93.75	93.75	93.75
Mass 4	100	87.50	100	93.75	100	100	100	100	100	100
Error	0.022	0.017	0.017	0.024	0.012	0.027	0.027	0.027	0.027	0.027

Figure 10 shows the integrated network output value compared with the predefined value. Each curve represents a fissile mass of the same output value, and there are five sets of samples for each mass. The sub-network identification results are given in Table 3. Comparing the integrated network output value with the default value, they can basically keep pace, and the average identification rate reaches 90%. So, we can identify different fissile mass with Elman neural network by using autocorrelation function as the input vector.

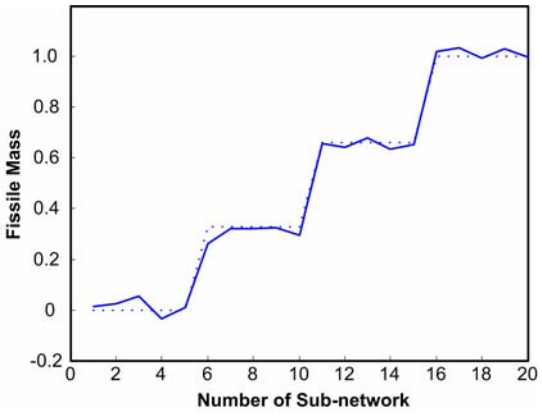

Fig.10 Identification results (solid line) *vs.* predefined value (dashed line).

5 Conclusion

Experiments were conducted to obtain key parameters of the HORNA system at different angles, source-detector distances and block sizes. Neutron signal data were acquired by three high-speed synchronized channels at sampling rate of 1 GHz. All the time- and frequency-dependent parameters, including auto/cross correlation functions, auto/cross power spectral density functions, coherence functions and ratio of power spectral density, were calculated and analyzed using block correlation and periodogram methods. Based on these, simulated autocorrelation functions of different fissile mass were generated and utilized for identification with an Elman neural network. Although experiments results show that the R_{psd} remains at approximately constant amplitude at ≤100 MHz, and is only related to the detector angle and source-detector distance, we still need more data and make more experiments to verify why the average value of R_{psd} is a bit smaller than the theoretical result. The trained Elman neural network could distinguish characteristics of the autocorrelation function and recognize different fissile mass. The average recognition rate reached 90% with high robustness.

Acknowledgments

The authors would like to thank the reviewers for their comments and Dr. Li Leilei for his help to improve the manuscript.

References

1 Luo Z L, Luo A R. Physics of experimental reactor. Beijing: Atomic Energy Press, 1987 (in Chinese).

2 Ding D Z, Ye C T, Zhao Z X. Neutron physics: principle, method and appliance. Beijing: Atomic Energy Press, 2001 (in Chinese).

3 Liu C A, Wu J. Nuclear arms control and verification technology concept. Beijing: National Defense Industry Press, 2007 (in Chinese).

4 Mihalczo J T, Mullens J A, Mattingly J K. Tthe U.S. Department of Energy Report No.: Y/LB-15946-R3, 1997, 1–43.

5 Mattingly J K, March-Leuba J A, Mihalczo J T. The U.S. Department of Energy Report No.: Y/LB-15971, 1998, 1–31.

6 Mihalczo J T, Blackman E D, Ragan G E, *et al.* Nucl Sci Eng, 1990, **104:** 314–338.

7 Mullens J A, Mattingly J K, Mihalczo J T. The U.S. Department of Energy Report No.: Y/LB-15968, 1998, 1–23.

8 Zhou B C, He B, Zhu W K, At Energy Sci Technol, 2006, **40:** 85–88 (in Chinese).

9 Hao F H, Hu G C, Liu S P. Chin J Phys, 2005, **54:** 3523–3529

10 Ren Y, Wei B Mi D L. J Chongqing Univ, 2009, **32:** 1054–1058 (in Chinese).

11 Wei B, Ren Y, Feng P. High Power Laser Particle Beams, 2009, **21:** 1898–1902 (in Chinese).

12 Jin J, Wei B, Feng P. High Power Laser Particle Beams, 2010, **22:** 2441–2447 (in Chinese).

13 Elman J L. Cogn Sci, 1990, **14:** 179–211.

14 Cecconi F, Campenni M. Proceedings of the Artificial Intelligence and Applications, 2006, 216–221.

15 Mihalczo J T. Nucl Sci Eng, 1974, **53:** 393–414.

16 Mihalczo J T. Blakeman E D, Ragan G E, *et al.* Nucl Technol, 1990, **94:** 336–360.